Effective thermal conductivity of a wet porous medium – Presence of hysteresis when modeling the spatial water distribution for the pendular regimé

Edouard Canot, Renaud Delannay, Salwa Mansour, Mohamad Muhieddine, Ramiro March

▶ **To cite this version:**

HAL Id: hal-01245690

https://inria.hal.science/hal-01245690

Submitted on 17 Dec 2015

Effective thermal conductivity of a wet porous medium – Presence of hysteresis when modeling the spatial water distribution for the pendular regime

Édouard Canot
CNRS researcher, IRISA
Campus de Beaulieu, Rennes (Fr)
Email: edouard.canot@irisa.fr

Renaud Delannay
Professor, IPR
Campus de Beaulieu, Rennes (Fr)
Email: renaud.delannay@univ-rennes1.fr

Salwa Mansour
PhD student, INRIA
Campus de Beaulieu, Rennes (Fr)
Email: salwa.mansour@inria.fr

Mohammad Muhieddine
Associate professor, Lebanese University
Nabatieh campus section V (Lb)
Email: mohamad.muhieddine@liu.edu.lb

Ramiro March
CNRS researcher, CreAAH
Campus de Beaulieu, Rennes (Fr)
Email: ramiro.march@univ-rennes1.fr

This paper deals with the heat transfer between two spherical grains separated by a small gap; dry air is located around the grains and a liquid water meniscus is supposed to be present between them. This problem can be seen as a micro-scale cell of an assembly of solid grains, for which we are looking for the effective thermal conductivity. For a fixed contact angle and according to the volume of the liquid meniscus, two different shapes are possible for the meniscus, giving a "contacting" state (when the liquid makes a true bridge between the two spheres) and a "non-contacting" one (when the liquid is split in two different drops, separated by a thin air layer); the transition between these two states occurs at different times when increasing or decreasing the liquid volume, thus leading to a hysteresis behavior when computing the thermal flux across the domain.

Keywords: *Effective thermal conductivity, Heat transfer, Granular porous medium, Water meniscus, Pendular regime, Fourier law, Humidity.*

1 Introduction

Transport phenomena in porous media have been investigated for over 100 years for applications in materials, agriculture, archeology and engineering. Recently, more interest has been focused on heat and mass transfer processes in micro-porous media due mainly to their increasing importance in functional material design, fuel cell optimization and even biomedical engineering [1, 2].

The effective thermal conductivity is one of the most important parameters characterizing the energy transport properties of porous media and has been studied extensively by using both theoretical and experimental approaches. As is well known, the effective thermal conductivity of porous media depends not only on the thermal property and the volume fraction of each constitute component, but on the microstructure (*i. e.* the spatial distribution of all components) of the media as well. On the other hand, it is known that the presence of water affects a lot the thermal properties because the thermal conductivity of water is about 25 times that of dry air. This has been mentioned by Chen [3] who emphasized that a small increment in water contents around the contact points will lead to rapid increment in the effective thermal conductivity. Some papers [4, 5] deal with the prediction of thermal conductivity in terrestrial soil media in the presence of liquid water as a component but without specifying its spatial localization. The paper [6] of Mitarai and Nakanishi concerns the pendular regime (see figure 1) in which the liquid content is small and where the water menisci form bridges at each contact point (between the grains) thus inducing two-body cohesive force so the study was restricted to the mechanical properties and not the thermal ones.

In this work, we consider a granular media constituted by solid grains which are more or less spherical in shape.
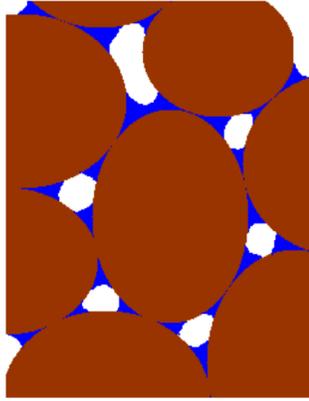
Fig. 1. Real granular medium in the "pendular regime": dry air is located around the grains (in white) whereas liquid water menisci (in blue) are present as liquid bridges between them.

change in the liquid volume.

Fig. 2. Simplification of the grains' assembly. The dashed rectangle is the computational domain used in this paper.

Four regimes of liquid content have been distinguished by [7]: Pendular, Funicular, Capillary and Slurry regimes. We are concerned with the pendular regime where we have a small liquid content and where the liquid bridges are formed at the contact points of grains due to the surface tension responsible for tendency of liquids to minimize their surface area, giving rise to a membrane-like surface [8].

Figure 1 represents a real granular medium in pendular regime. This three component medium has no theoretical model to calculate the effective thermal conductivity and it is difficult to be discovered by experimental results. However, a numerical value of this effective property can be found in two stages, that is to say first finding the equilibrium shape of the liquid meniscus for a given liquid volume, second solving the steady-state heat equation over a small domain (supposed to be representative enough of the whole domain) and deduce the effective thermal conductivity, via the Fourier law, by using the thermal flux through the domain.

In this paper, we focus on the heat transfer between two spherical solid grains of same radius in presence of dry air and where liquid water is attached to the solid grains, without gravity. Our model takes into account the role of the contact angle between the liquid-gas interface in addition to the surface tension (energy required to increase the surface area of a liquid by a unit area) which enable the calculation of the exact shape of the liquid meniscus. A simplification of the grains' assembly is represented in figure 2.

The present model implies many assumptions; there is no doubt that some important characteristics of a real granular medium (especially the randomness of both shape and position of the grains, and the roughness of their surface) should affect the results obtained in this paper. On the other hand, we can state that gravity doesn't affect a lot the shape of the liquid menisci (the Bond number, based on a reference length chosen as the height of the meniscus, is of the order of one thousandth for a grain of radius 1 *mm*). Nevertheless, we think that our simple model has the worthiness to reveal a very interesting behavior, that is the hysteresis during the
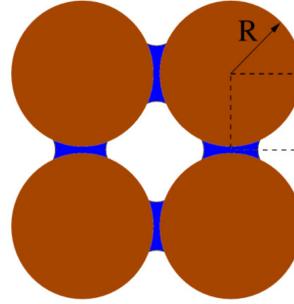
2 Micro-scale Model

We want to solve the steady-state heat transfer in an elementary cell containing only two spherical solid grains, a few quantity of liquid water, and dry air. In a real situation, the liquid water should be in thermodynamic equilibrium with its vapor, so the surrounding gas should be a binary mixture of dry air and water vapor. In the present study, the water vapor is neglected and we assume that there is no adsorbed water on the grain surface. The computational domain (see figure 3) can be found using the symmetry planes of the problem knowing the main direction of the heat flux – for example, the bottom symmetry plane comes from the fact that the gravity is neglected. Top and bottom sides are kept at constant (but different) temperature whereas the vertical ones are supposed to be isolated (this is related to the model used by [3] in their study of thermal conduction in dry soils).

As stated in the introduction, the liquid meniscus is centered along the axis between the two spheres leading to an axi-symmetric problem, so we can reduce the geometrical independent variables to the (r, z) cylindrical coordinates. Each component (solid, liquid water and dry air) has a constant thermal conductivity and the thermal contact between the components is supposed to be perfect.

Because it is in mechanical equilibrium (actually, in a quasi-static state because in a real situation a change of volume can be expected due to many reasons), the shape of the liquid meniscus must have both a constant total curvature (it is a minimum surface) and a prescribed contact angle with the solid. The percentage of liquid water, *i. e.* the ratio of its volume to that of the available space between the spheres is called humidity.

The input parameters are:

R : the radius of the two solid spheres
ε : half the gap between the spheres
V : the volume of liquid water
γ : the surface tension between liquid water and air
θ : the contact angle between the liquid interface and the solid
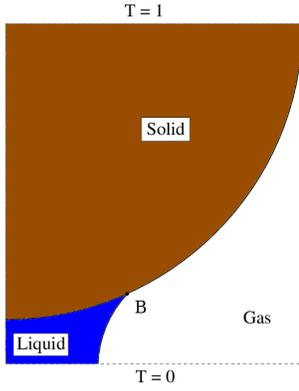
Fig. 3. Sketch of the cylindrical computational domain (taking into account all the symmetries). Boundary conditions are of homogeneous Dirichlet type on top and bottom sides, and of zero Neumann type on the external vertical sides.

In this study, the radius R is taken as the reference length. The output variable of the problem is the (vertical) flux q across the domain which is related to the effective thermal conductivity of our composite medium (by Fourier law). Note that in a complete model, the liquid volume V should be related to the gas pressure (in a real situation, the total mass of the water is fixed and then the repartition between gas and liquid depends on the local pressure) but this is out of the scope of this study.

Surface tension γ and contact angle θ are usually temperature dependent and this dependence (which can be found elsewhere in literature) is not so negligible. However, at the scale of our elementary cell, we can state that the temperature difference is small so that these two parameters can be treated as constants.

3 Equilibrium shape of the liquid meniscus

In physics, the Young-Laplace equation relates the pressure difference to the shape of the interface [9]:

$$\Delta P = \gamma \kappa \qquad (1)$$

where ΔP is the pressure difference across the fluid interface, γ is the surface tension and κ is the total curvature. At micro-scale, ΔP has a constant value and this could be easily demonstrated using the hydrostatic equation. Moreover, γ is supposed to remain constant so according to equation (1), κ is constant as well.

$$\kappa = \kappa_1 + \kappa_2 = \text{constant} \qquad (2)$$

where κ is the total curvature of the liquid meniscus curve (C) and κ_1 and κ_2 are respectively its plane and axi-symmetric curvatures.

Let $\{r(s), z(s)\}$ be any parameterization of the curve (C) in the axi-symmetric cylindrical coordinates then the total curvature is given by:

$$\kappa = \frac{r'z'' - z'r''}{(r'^2 + z'^2)^{\frac{3}{2}}} + \frac{z'}{r} \qquad (3)$$

where $z' = dz/ds$, $r' = dz/ds$, $z'' = d^2z/ds^2$ and $r'' = d^2r/ds^2$. If we choose s such that it corresponds to the arc length parameterization of curve (C) then:

$$r'^2 + z'^2 = 1 \qquad (4)$$

and thus equation (3) becomes:

$$r'z'' - z'r'' + \frac{z'}{r} = \kappa \qquad (5)$$

The geometrical shape of the liquid meniscus is obtained by integrating the differential algebraic system formed of equations (4) and (5) (indeed, after transforming the system in a first order type, the former equation appears under an algebraic form).

Regarding the initial conditions for this integration, the following explanation should be emphasized: we already mentionned in section 2 that both the volume V and the contact angle θ was chosen as an input parameters; actually, it is difficult to integrate the meniscus shape (equations (4-5)) under these two constraints. We have preferred instead to define a point in the (r, z) plane (point A in figure 4) which is the beginning of the integration; the integration is then stopped when the meniscus curve crosses the solid boundary, (point B in figure 4). Please note that the point A is located on the r-axis only for the "contacting" case; for the "non-contacting" case, the point A must be located on the z-axis. The constraint concerning the prescribed contact angle at B, on the contrary, is kept and the integration process is repeated by trial and error until obtaining the good contact angle.

To summarize, the initial conditions for the integration of (4-5) are as follows:

$$\text{"contacting" case:} \begin{cases} r = r_0 \\ z = 0 \\ z' = 0 \end{cases}$$

$$\text{"non-contacting" case:} \begin{cases} r = 0 \\ z = z_0 \\ r' = 0 \end{cases}$$

It is worth noting that since the contact angle is prescribed, the total curvature κ and the meniscus volume V

are conjugates in the sense where the knowledge of one of them leads to that of the other. If we choose a value of V, the differential system (4-5) will be difficult to be integrated, because of the presence of two constraints: the contact angle θ and the liquid volume V. To simplify the integration, we prefer to choose a value of the total curvature κ and deduce the volume V (the computation is detailed afterwards). Anyway, the final curves of the thermal fluxes will be plotted with respect to the volume V, as a control parameter.

3.1 The volume of the liquid water V

Figure 4 is a sketch used to demonstrate the calculation of the volume of liquid water V. The volume of the hashed slice of height dz is $\pi r(z)^2 dz$ so the volume of both the blue and the brown parts is $V_b = \int_{z_A}^{z_B} \pi r(z)^2 dz$. Earlier, we have found the values of $r(s)$ and $z(s)$ so by a simple change of variable we can say that the volume of these two parts can be written in the form $V_b = \int_{s_A}^{s_B} \pi r(s)^2 \dfrac{dz}{ds} ds$ and hence:

$$\frac{dV_b}{ds} = \pi r(s)^2 \frac{dz}{ds} \tag{6}$$

Equation (6) is actually added to the system of equations (4-5) and therefore V_b is a result of the integration process. To find the volume of liquid water V we must subtract the volume of the spherical cap V_c (in brown) which is given by: $V_c = \dfrac{\pi h^2}{3}(3R - h)$ where $h = z_B - \varepsilon$ and $R = 1$ (radius of the grain). Finally, $V = V_b - V_c$.
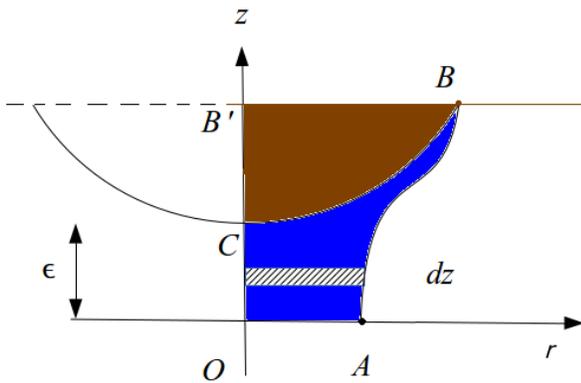
Fig. 4. A scheme of the liquid meniscus (solid grain in brown and liquid water in blue). A is an arbitrary point defined as the beginning of the integration process.

3.2 The contact angle θ between liquid and solid interface

Figure 5 is a sketch to demonstrate the calculation of the liquid and solid interface contact angle θ. Based on the

knowledge of the position (r_B and z_B) of point B and the intersection point between the liquid water and the solid grain, we can easily calculate θ. Let ψ be the angle formed by the tangent to the liquid meniscus at B then $\psi = arctan(z'_B/r'_B)$ (the prime denotes the derivative w.r.t. the curvilinear abscissa s) and assume that φ is the angle formed by the tangent to the solid grain at B then $\varphi = arcsin(r_B/R)$. Simply $\theta = \psi - \varphi$.
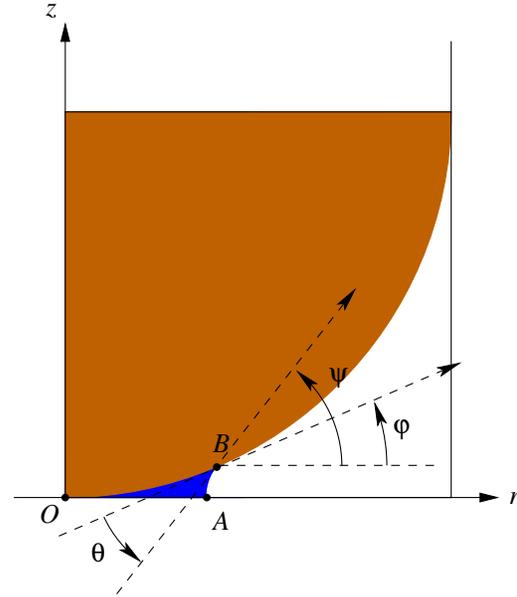
Fig. 5. A zoom of the liquid-solid interface (solid grain in brown and liquid water in blue).

The solution of our system of equations (4-5) is obtained numerically by a shooting method over the starting position of the integration (r_0 in the "contacting" state or z_0 in the "non-contacting" state); this starting position is varied until the prescribed contact angle θ is found. The family of the curves obtained when we vary the total curvature κ, is drawn in figures 6 and 7 for the two states.

4 Numerical Computation of the heat flux

Solving our problem numerically appears unavoidable: some authors (resp. [10, 11]) have used analytical solutions but they are respectively restricted to an asymptotic behavior (so, adapted to a local geometrical zone) or to too crude approximations.

Consider the steady state heat equation in 3D axisymmetric cylindrical coordinates:

$$\frac{1}{r}\frac{\partial}{\partial r}\left(k(r,z)\, r\, \frac{\partial T}{\partial r}\right) + \frac{\partial}{\partial z}\left(k(r,z)\, \frac{\partial T}{\partial z}\right) = 0 \tag{7}$$

with homogeneous Dirichlet boundary conditions on top and bottom sides and zero Neumann boundary conditions (i.e. isolated conditions) on the external vertical sides. This
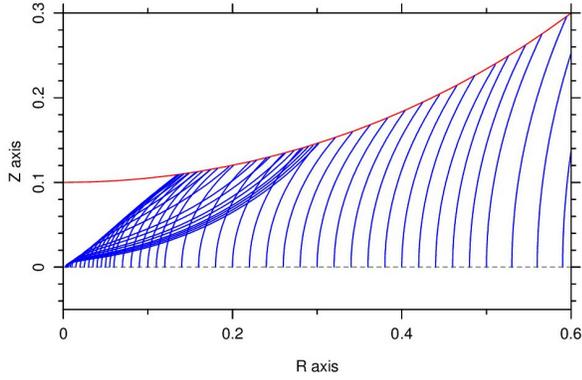
Fig. 6. This represents the family of the liquid meniscus when the volume varies, in the "contacting" state. Each curve is the boundary of the half of a bridge linking the two grains.
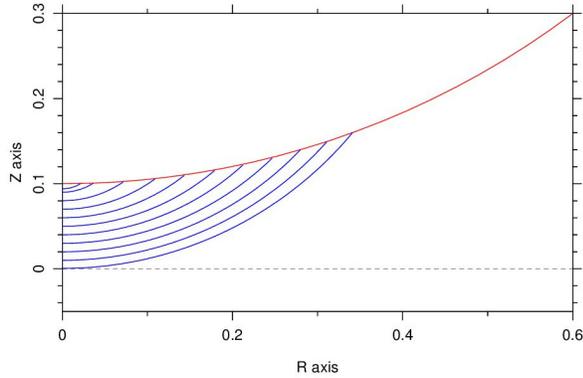

Fig. 7. This represents the family of the liquid meniscus when the volume varies, in the "non-contacting" state. Each curve is the boundary of a sessile drop, and the same symmetric drop is on the top of the other grain (not represented).

steady state equation is solved using a Finite Volume scheme applied on a regular structure mesh of rectangular cells. The detailed discretization over an interior cell with node (i, j) is explained below:

$$\int_{i-\frac{1}{2}}^{i+\frac{1}{2}} \int_{j-\frac{1}{2}}^{j+\frac{1}{2}} \frac{1}{r} \frac{\partial}{\partial r}\left(k(r,z)\, r \,\frac{\partial T}{\partial r}\right) r\, dr\, dz$$

$$= \left(\frac{k_{i,j}+k_{i+1,j}}{2}\frac{r_i+r_{i+1}}{2}\frac{T_{i+1,j}-T_{i,j}}{\Delta r}\right.$$

$$\left. -\frac{k_{i,j}+k_{i-1,j}}{2}\frac{r_i+r_{i-1}}{2}\frac{T_{i,j}-T_{i-1,j}}{\Delta r}\right)\Delta z$$

and

$$\int_{i-\frac{1}{2}}^{i+\frac{1}{2}} \int_{j-\frac{1}{2}}^{j+\frac{1}{2}} \frac{\partial}{\partial z}\left(k(r,z)\,\frac{\partial T}{\partial z}\right) r\, dr\, dz$$

$$= \left(\frac{k_{i,j}+k_{i,j+1}}{2}\frac{T_{i,j+1}-T_{i,j}}{\Delta z}\right.$$

$$\left. -\frac{k_{i,j}+k_{i,j-1}}{2}\frac{T_{i,j}-T_{i,j-1}}{\Delta z}\right)r_i\,\Delta r$$

where Δr and Δz represents the distance between two consecutive nodes in the r and z directions respectively. $k_{i,j}$ is the value of the conductivity at the node of the specified cell — a geometric test is done to specify the nature of the cell (solid, water or air) to specify the value of the conductivity at the requested cell.

After writing the discretization on the other boundary cells, the equations will be written as a linear system and the matrix of this linear system is stored in a sparse way and the UMFPack linear sparse solver is used. Some tries have shown that a 500 by 500 mesh is required to obtain a good accuracy (see figure 9). Each numerical computation takes about few seconds on a laptop (Intel Core i7 @ 2.7 GHz).

Now we have obtained by numerical simulations the value of the temperature at the node of each cell. To calculate the heat flux that flows through our domain, we need to sum up the flux that flows through each cell on the top boundary (for example). Let (i, j) be the node of a non-corner top boundary cell (see figure 8).
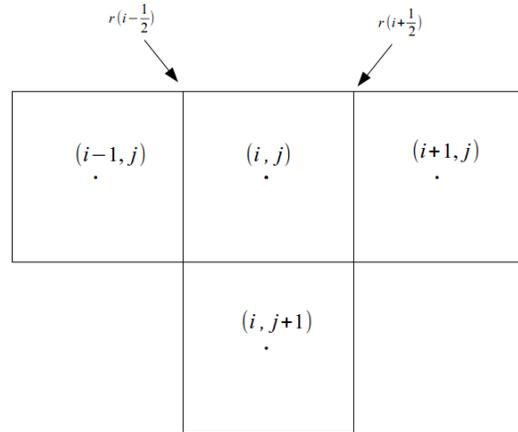

Fig. 8. A representation of a top (non-corner) cell with its neighbor cells.

The temperature gradient at cell $(i, 1)$ (top boundary cell for which $j = 1$) is given by:

$$\left.\frac{\partial T}{\partial z}\right|_i = \frac{T_{i,1} - T_{i,2}}{z_2 - z_1}$$

Recall that $r_{i+\frac{1}{2}} = \dfrac{r_i + r_{i+1}}{2}$ and $r_{i-\frac{1}{2}} = \dfrac{r_i + r_{i-1}}{2}$ so the flux that flows through the cell with node $(i, 1)$ is:

$$q_i = \pi \frac{k_{i,1} + k_{i,2}}{2}\left.\frac{\partial T}{\partial z}\right|_i \left(r_{i+\frac{1}{2}}^2 - r_{i-\frac{1}{2}}^2\right) \qquad (8)$$

Finally, to calculate the total flux which flows through our computational domain we add up the flux at each top-border cell.
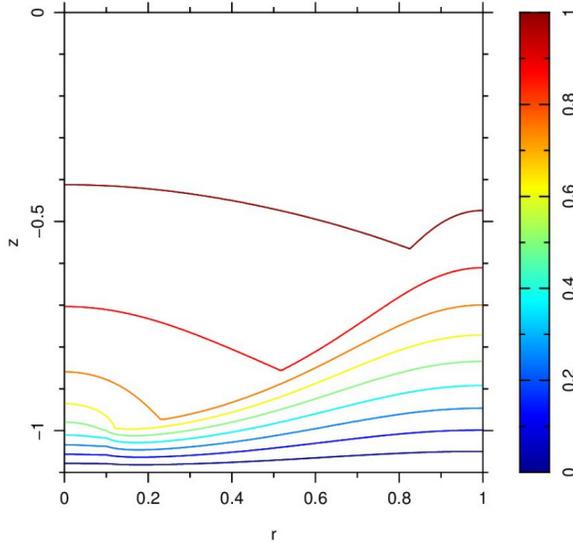
Fig. 9. Example of contour curves of the temperature obtained after a numerical computation on a 500x500 mesh, in the case $\varepsilon/R = 0.1$, $\theta = 30$ deg. Due to Dirichlet boundary condition (bottom: $T = 0$ and top: $T = 1$), each contour line from bottom to top corresponds to the temperature: $T = 0.1, 0.2, ..., 0.9$ respectively.

5 Heat flux with respect to water liquid volume

During the evaporation/condensation of water in a wet granular medium, the liquid volume in each elementary cell changes with time. It is interesting to know the variation of the effective thermal conductivity with respect to the liquid volume. By using the Fourier law on our computational domain, the effective thermal conductivity is proportional to the heat flux. This heat flux depends of course on the water liquid volume because, as stated in the introduction, the thermal conductivity of the water is much more important than that of the dry air. Further, we expect a jump in the

heat flux curve because there are two possible geometrical configurations for the liquid meniscus (the "contacting" state and the "non-contacting" one, as described in figures 6 and 7).

The numerical values are the following:

thermal conduct. of water $k_w = 0.61\ W\,m^{-1}\,K^{-1}$
thermal conduct. of dry air $k_a = 0.024\ W\,m^{-1}\,K^{-1}$
thermal conduct. of solid $k_s = 1.52\ W\,m^{-1}\,K^{-1}$
radius of the grains $R = 1 \times 10^{-3} m$
surface tension of water $\gamma = 72 \times 10^{-3} N\,m^{-1}$

The computed heat flux is presented in figure 10, for humidity (or liquid fraction, which is the ratio of the liquid volume divided by the void volume) ranged from 0 to 0.18. As expected, a hysteresis behavior is highlighted by our numerical computations and is more visible in figure 11 which presents an enlarged view of the previous one.
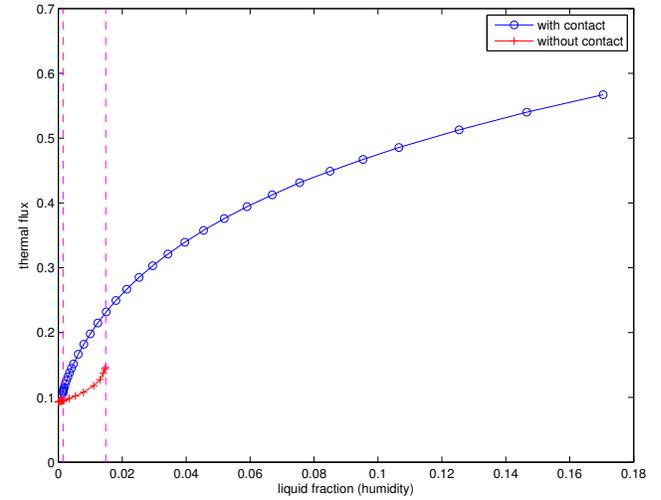

Fig. 10. Thermal heat flux w.r.t. the liquid fraction, for the "contacting" state (blue) and the "non-contacting" state (red). $\varepsilon/R = 0.1$, $\theta = 30$ deg. Note the great increase in the heat flux due to the presence of water: about a factor of 5 when humidity is only 0.12.

Once the heat flux through the computational domain has been obtained, it could be very easy to deduce the effective thermal conductivity k_e by using the Fourier law applied in a global manner to our domain. Actually k_e is proportional to the heat flux so it is not necessary to present the numerical results for k_e, as the main objective of this paper is to focus on the hysteresis behavior.

The role of the parameters ε and θ is summarized in table 1. Refering to figure 11, we characterize the hysteresis by defining the two following quantities:

- the *Hysteresis Length* which is the dimension of the hysteresis cycle along the *x*-axis;
- the *Flux jump* which is the other dimension along the *y*-axis.
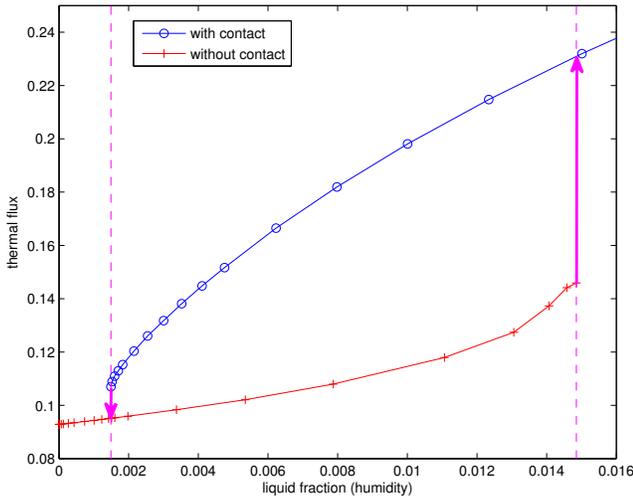
Fig. 11. This zoom of figure 10 shows with more evidence the hysteresis behavior when liquid fraction is increasing or decreasing. The jump in the heat flux occurs at the magenta dashed line; this jump is more pronounced in the increasing case, *i. e.* when liquid water increases. The arrows show the direction in the hysteresis cycle.

Table 1. Role of sphere distance ε and contact angle θ on the hysteresis

ε/R	θ (degree)	Hysteresis Length	Flux jump
0.05	10	0.0192	0.165
0.05	30	0.002027	0.041026
0.05	45	0.0008265	0.021695
0.1	10	0.10684	0.285
0.1	30	0.013434	0.0881
0.1	45	0.005633	0.048

Table 1 shows that the hysteresis is more and more pronounced as the distance ε increases. Moreover, it is more pronounced for small contact angles. In the extreme geometrical situation where the distance ε is zero (the solid spheres are contacted themselves) the hysteresis disappears because we obtain always the "contacting" state.

Figure 12 (resp. 13) shows the variations of the heat flux curves with respect to the distance ε (resp. wrt θ). They show clearly that the influence of the distance ε is more important than that of the contact angle θ.

6 Conclusion

A strong hysteresis behavior for the effective thermal conductivity has been revealed when changing the humidity of a granular medium. It is due to a switch between two different geometrical configurations of the liquid meniscus attached to the two solid spheres as a bridge. In real situa-
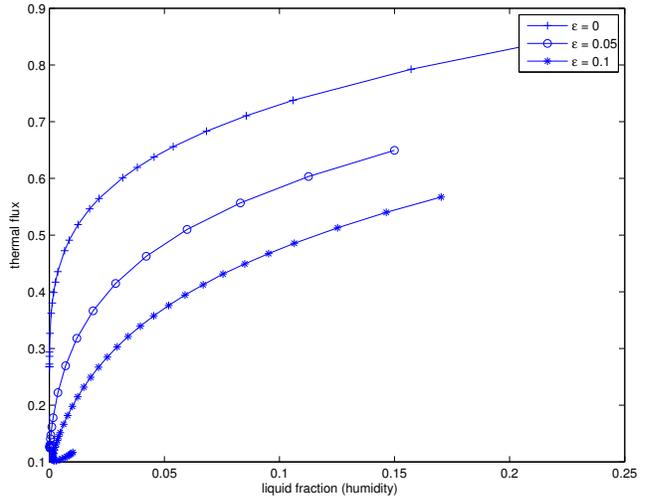
Fig. 12. Thermal heat flux w.r.t. the liquid fraction, for the "contacting" state only, when $\theta = 30$ deg. The curves show the influence of the distance ε.
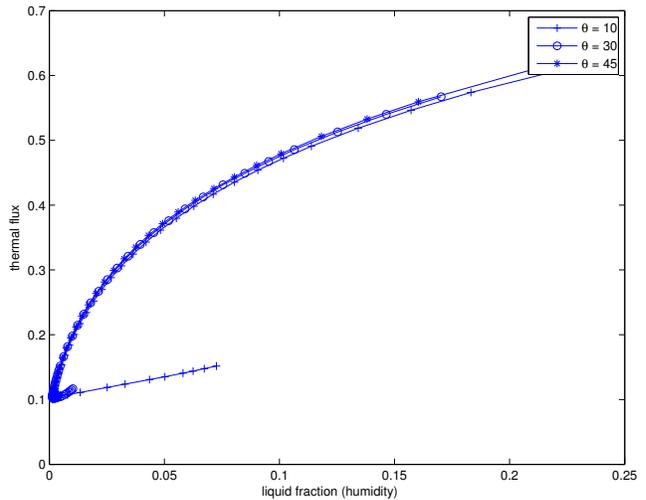
Fig. 13. Thermal heat flux w.r.t. the liquid fraction, for the "contacting" state only, when $\varepsilon/R = 0.1$. The curves show the influence of the contact angle θ.

tions, this hysteresis behavior should remain present, despite its attenuation due the randomness characteristics of both the shape and position of the grains.

In this study, the heat transfer has been restricted to the conduction phenomenon. It is evident that, according to the problem treated, other types of transfer should be taken into account, such as *e. g.* latent heat due to evaporation/condensation at the gas-liquid interface, or radiation. This may be included in a future work.

References

[1] Ingham, D. B., and Pop, I., 2005. *Transport Phenomena in Porous Media III*. Elsevier, Oxford, UK.

[2] Bejan, A., 2004. "Design porous media". In Emerging Technologies and Techniques in Porous Media, D. B. Ingham, A. Bejan, E. Mamut, and I. Pop, eds., Kluwer, London, pp. 337–349.

[3] Chen, S. X., 2008. "Thermal conductivity of sands". *Heat Mass Transfer,* **44**, pp. 1241–1246.

[4] Usowicz, B., Lipiec, J., Marczewski, W., and Ferrero, A., 2006. "Thermal conductivity modelling of terrestrial soil media – a comparative study". *Planetary and Space Science,* **54**, pp. 1086–1095.

[5] Yun, T. S., and Santamarina, J. C., 2008. "Fundamental study of thermal conduction in dry soils". *Granular Matter,* **10**, pp. 197–207.

[6] Mitarai, N., and Nakanishi, H., 2009. "Simple model for wet granular materials with liquid clusters". *Europhysics Letters,* **88**, pp. 1–6.

[7] Mitarai, N., and Nori, F., 2006. "Wet granular materials". *Adv. Phys.,* **55**, pp. 1–45.

[8] Tro, N. J., 2011. *Chemistry: A Molecular Approach.* Prentice Hall.

[9] Guyon, É., Hulin, J.-P., Petit, L., and Mitescu, C., 2001. *Physical Hydrodynamics.* Oxford University Press.

[10] Batchelor, G. K., and O'Brien, R. W., 1977. "Thermal or electrical conduction through a granular material". *Proc. of Royal Society of London A,* **355**, pp. 313–333.

[11] Garrett, D., and Ban, H., 2011. "Compressive pressure dependent anisotropic effective thermal conductivity of granular beds". *Granular Matter,* **13**, pp. 685–696.

List of Figures

List of Tables